molecules

MDPI

Article

Synthesis and Characterizations of Zinc Oxide on Reduced Graphene Oxide for High Performance Electrocatalytic Reduction of Oxygen

Jiemei Yu [1,2], Taizhong Huang [2], Zhankun Jiang [2], Min Sun [2,*] and Chengchun Tang [1,*]

[1] School of Materials Science and Engineering, Hebei University of Technology, 8 of First Road of Dingzigu, Hongqiao District, Tianjin 300130, China; chm_yujm@ujn.edu.cn

[2] School of Chemistry and Chemical Engineering, University of Jinan, 336 West Nanxinzhuang Road, Jinan 250022, China; chm_huangtz@ujn.edu.cn (T.H.); chm_jiangzk@ujn.edu.cn (Z.J.)

* Correspondence: chm_sunm@ujn.eud.cn (M.S.); tangcc@hebut.edu.cn (C.T.); Tel: +86(0)-15053123169 (M.S.)

Received: 15 November 2018; Accepted: 4 December 2018; Published: 6 December 2018

Abstract: Electrocatalysts for the oxygen reduction (ORR) reaction play an important role in renewable energy technologies, including fuel cells and metal-air batteries. However, development of cost effective catalyst with high activity remains a great challenge. In this feature article, a hybrid material combining ZnO nanoparticles (NPs) with reduced graphene oxide (rGO) is applied as an efficient oxygen reduction electrocatalyst. It is fabricated through a facile one-step hydrothermal method, in which the formation of ZnO NPs and the reduction of graphene oxide are accomplished simultaneously. Transmission electron microscopy and scanning electron microscopy profiles reveal the uniform distribution of ZnO NPs on rGO sheets. Cyclic voltammograms, rotating disk electrode and rotating ring disk electrode measurements demonstrate that the hierarchical ZnO/rGO hybrid nanomaterial exhibits excellent electrocatalytic activity for ORR in alkaline medium, due to the high cathodic current density (9.21×10^{-5} mA/cm^2), positive onset potential (-0.22 V), low H_2O_2 yield (less than 3%), and high electron transfer numbers (4e from O_2 to H_2O). The proposed catalyst is also compared with commercial Pt/C catalyst, comparable catalytic performance and better stability are obtained. It is expected that the ZnO/rGO hybrid could be used as promising non-precious metal cathode in alkaline fuel cells.

Keywords: non-precious-metal catalyst; oxygen reduction reaction; zinc oxide; reduced graphene oxide

1. Introduction

The oxygen reduction reaction (ORR) at the cathode plays crucial rule in energy transformation, for it enables various energy technologies to achieve large energy densities, including water splitting, metal-air batteries and fuel cells [1,2]. Over the past decades, Pt-based catalysts have shown the best catalytic performance for ORR. Nevertheless, such materials suffer from poor reliability and durability problems (e.g., poisoning and crossover effects), as well as the low abundance and the increasing cost of platinum, which has constrained their large-scale commercial application [3–5]. Thus, searching for cheap and abundant catalysts with excellent performance substituting for Pt is very important and necessary from the point view of sustainable development [6,7].

Graphene, one of conductive carbon matrices, has attracted continually attention because of its high surface area, superior electric conductivity, large surface area, good flexibility, and strong adhesion to catalytic particles [8–10]. With the unique surface chemistry and 2D microstructure, graphene has been proven to be an ideal platform for anchoring or growing guest species [11,12]. Thus, many new strategies for growing metal oxide layers on graphene nanosheets have been developed. Recent investigations have demonstrated that transition metal oxide nanoparticles (NPs) anchored

on graphene are one of the most promising ORR catalysts, which can substitute for Pt and Pt-based catalysts. Nitrogen-doped reduced graphene oxide supported cobalt oxide nanosheets [13], Co@CoO and acetylene black particles supported on the wrinkled nitrogen doped reduced graphene oxide (rGO) [14], Co_3O_4 nanosheets anchored on rGO-coated nickel foam [15], spinel $CoMn_2O_4$ doped reduced graphene oxide [16], (*N*,*F*)-codoped TiO_2 supported by rGO [17], and MnO_2 nanoparticles anchored on rGO [18] et al., have exhibited comparable electrocatalytic activity but superior stability toward ORR compared with the commercial Pt/C catalyst. These studies on transition metal oxides-graphene interactions revealed that depending on the metal-graphene spacing and the spinel structure of transition metal oxides, charge transfer may exist between the transition metal oxides and graphene, which may be the real reason that certain transition metal oxides NPs supported on graphene surface exhibit enhanced catalytic activities [19].

With the high desirability for seeking clean and efficient energy sources, there is still room for developing cost effective ORR catalysts with high catalytic properties. Among the transition metal oxides that have been investigated, Zinc oxide (ZnO), with its outstanding merits of high catalytic activity, non-toxicity and great chemical stability, has drawn particular attention [20,21]. Over the past decades, ZnO nanostructures have been explored for applications such as field effect transistors, ultra-violet light sources, piezoelectric nanogenerators, gas sensors, cold cathode electron sources and solar cells [22–24]. However, up to now there has been no report about ZnO serving as an efficient ORR catalyst. Considering the relatively poor electroconductivity of ZnO, which may greatly hinder its application as an electrode material in the oxygen reduction process, it is necessary to combine ZnO with rGO layers as oxygen reduction catalyst. Therefore, the electrocatalyst of ZnO NPs anchored on rGO was obtained through an extremely facile route in this paper. We hope it can be used as a highly efficient electrocatalyst.

2. Results and Discussion

2.1. Structural Characterization

Figure 1a shows the XRD (X-ray diffraction) patterns of ZnO and ZnO/rGO, the characteristic peak locates at 31.78°, 34.43°, 36.26°, 47.55°, 56.61°and 62.88°, corresponding to the (100), (002), (101), (102), (110) and (103) plane of ZnO with the hexagonal wurtzite phase (PDF: 01-089-0510), respectively [25]. No evidence of any impurities were detected. The XRD pattern of ZnO/rGO also shows an unconspicuous peak at around 24.2°, which related to the (002) plane of graphene, implying the removal of oxygenated functional groups during the reduction of GO into rGO. Figure 1b shows the Raman spectrum of ZnO/rGO. The D band (1350 cm^{-1}) is correlated to the disorders and structural defects of graphene, whereas the G band (1590 cm^{-1}) is corresponded to the sp^2-hybridized graphitic carbon atoms [26,27]. The relative intensity rations of D to G peak (I_D/I_G) for ZnO/rGO is 1.1, indicating the partially reduced of GO to rGO.

X-ray photoelectron spectroscopy (XPS) analyses were recorded to probe the elemental chemical states and the surface chemical composition of our samples. Figure 1c displays the survey spectra of ZnO and ZnO/rGO. As expected, Figure 1c clearly shows that the ZnO/rGO mainly contains the elements C, O and Zn. The C element of ZnO/rGO results from the adventitious element carbon and the rGO molecules, while in the ZnO spectrum, it only comes from the contamination of the testing environment. Figure 1d shows the C 1s spectrum of ZnO/rGO hybrid, which can be deconvoluted into three components identified as C-C (284.0 eV), C-O (286.0 eV) and C=O (287.5 eV), respectively. The Zn 2p spectrum of the ZnO (Figure 1e) and ZnO/rGO (Figure 1f) displays doublet peaks. The peak located at 1044.1 eV and 1021.5 eV are assigned to Zn $2p_{1/2}$ and $2p_{3/2}$ of Zn^{2+} in ZnO, while the corresponding peaks of Zn 2p in ZnO/rGO were observed at 1045.0 eV and 1022.4 eV, shifting towards the higher energy region by 0.9 eV [28]. The O 1s XPS spectrum of ZnO and ZnO/rGO is shown in Figure 1g,h. As seen in Figure 1g, the peaks located at 530.1 eV and 532.3 eV correspond to O^{2-} ions in the Zn-O species and the oxygen-deficient regions of the wurtzite ZnO structure, respectively [29]. The peak

located at 534.1 eV is related to the OHs or oxygen groups absorbed onto the surface of the catalyst [30]. The corresponding O 1s peaks in ZnO/rGO are located at 530.3 eV, 532.5 eV and 534.2 eV. It should be mentioned that the peak intensities at 532.5 eV and 534.2 eV of ZnO/rGO are much stronger than that of pure ZnO, indicating the significant increase of OH or oxygen groups absorbed onto the surface of ZnO/rGO, compared with pure ZnO. The absorbed oxygen or OH groups may be helpful to enhance the electrocatalytic activity of ZnO/rGO [31,32].

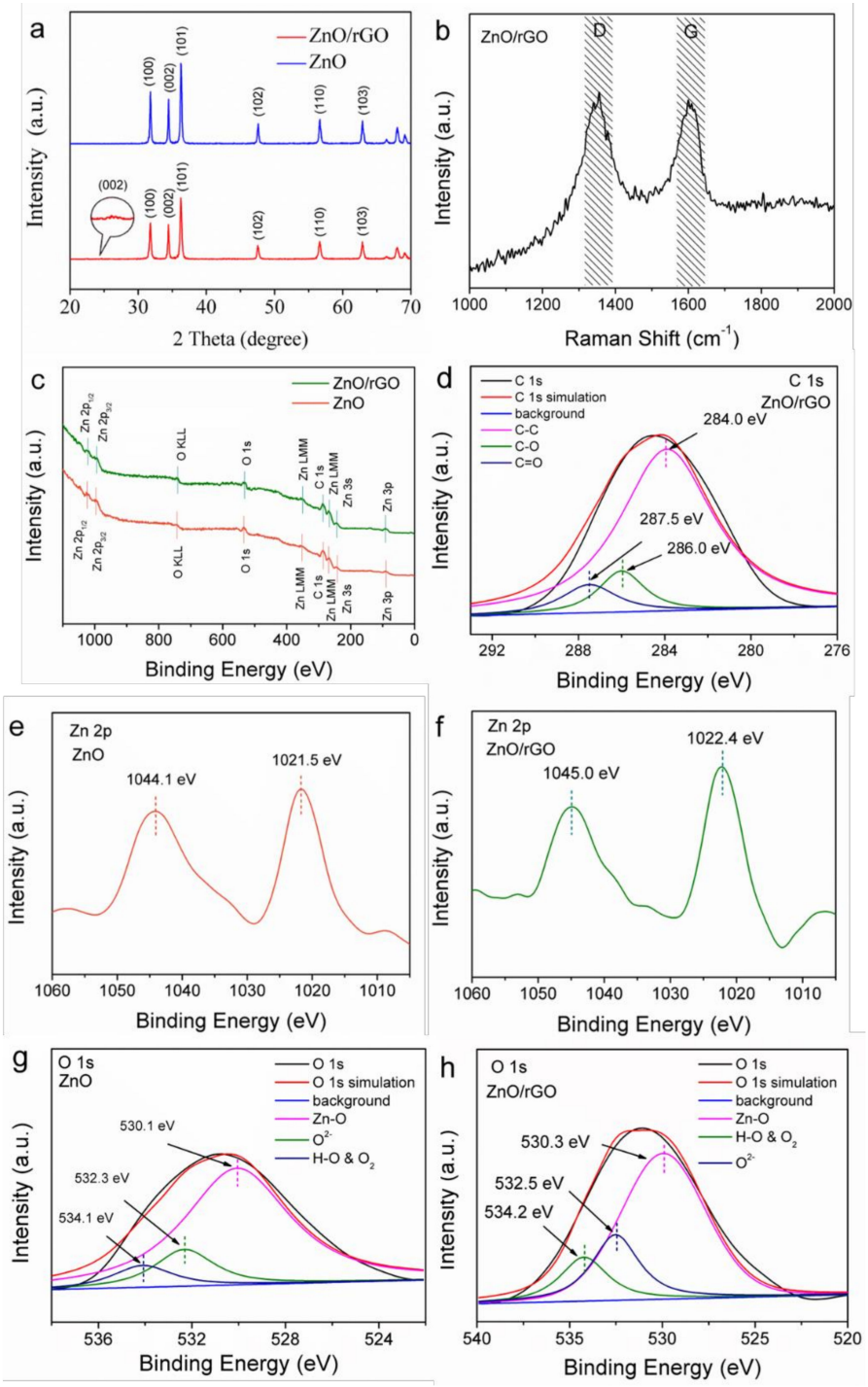

Figure 1. (**a**) X-ray diffraction patterns of ZnO and ZnO/rGO. (**b**) Raman spectrum of ZnO/rGO. (**c**) XPS survey spectra of ZnO and ZnO/rGO. Typical high-resolution XPS spectra of C 1s in ZnO/rGO (**d**), Zn 2p in ZnO (**e**) and ZnO/rGO (**f**). Typical high-resolution XPS spectra of O 1s in ZnO (**g**) and ZnO/rGO (**h**).

Figure 2a,b show typical scanning electron microscope (SEM) images of the obtained ZnO and ZnO/rGO hybrid. In Figure 2a, ZnO NPs are aggregated to a certain extent. While in Figure 2b, rGO nanosheets serve as the support frame, ZnO NPs attach onto it densely and uniformly. Figure 2c,e show the transmission electron microscopy (TEM) images of our samples. As shown in Figure 2c, the particle size of ZnO is about 9.5 nm, while in Figure 2e, ZnO NPs are well dispersed on graphene sheets with a narrow particle size distribution of 6.5~8.5 nm. Note that ZnO NPs in ZnO/rGO are smaller than that of pure ZnO, due to the dispersing effect of rGO in preventing ZnO NPs from aggregation [33]. Figure 2d,f show the high resolution TEM (HRTEM) images of ZnO and ZnO/rGO, a clear lattice spacing of 0.28 nm, 0.25 nm and 0.19 nm can be observed, agrees well with the (100), (101) and (102) plane of hexagonal ZnO, respectively [34].

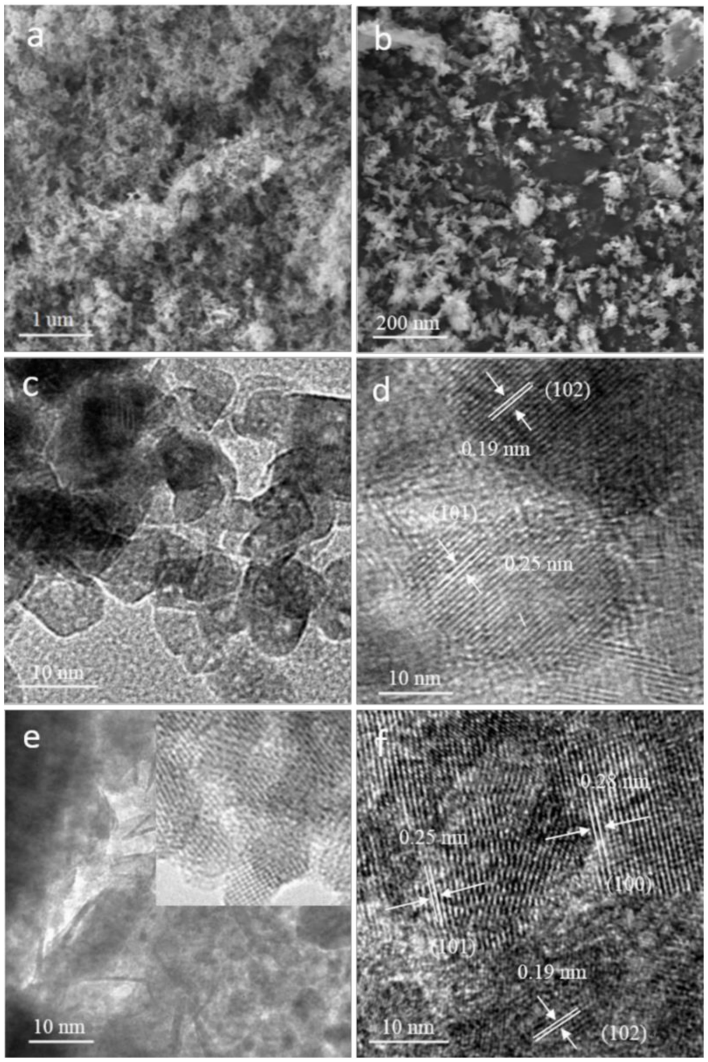

Figure 2. SEM images of (**a**) ZnO, (**b**) ZnO/rGO. TEM images of (**c**) ZnO and (**e**) ZnO/rGO. HRTEM images of (**d**) ZnO and (**f**) ZnO/rGO.

2.2. Electrocatalytic Activity towards Oxygen Reduction Reaction

The CV test was performed to evaluate the electro-activity of our samples in Ar and then in O_2-saturated 0.1 M KOH solution from 0.2 to 0.8 V at a scan rate of 5 mV/s vs. Hg/Hg_2Cl_2 reference electrode. As shown in Figure 3a–c, the CV tests of ZnO, rGO and ZnO/rGO are essentially featureless under an Ar atmosphere. There is no peak appearing at the rGO electrode in O_2-saturated electrolyte, either, indicating that rGO is inherently electrochemically silent under these conditions. A significant ORR peak is observed in ZnO and ZnO/rGO under an O_2 atmosphere. Remarkably, ZnO/rGO exhibits

a higher cathodic current density and a more positive ORR onset potential (−0.2 V vs. −0.24 V for ZnO) compared with ZnO (Figure 3d). The improved catalytic activity of ZnO/rGO can be attributed to the presence of rGO nanosheets, which improve the electrical conductivity of ZnO/rGO by providing a rapid electron transfer access [18]. The Tafel test results of ZnO and ZnO/rGO are illustrated in Figure 3e. The Tafel slopes are calculated to be 189 mV/dec and 133 mV/dec for ZnO and ZnO/rGO, respectively. It is obvious that the Tafel slope of ZnO/rGO is smaller than that of ZnO, the lower Tafel slope indicates the higher intrinsic catalytic activity [35].

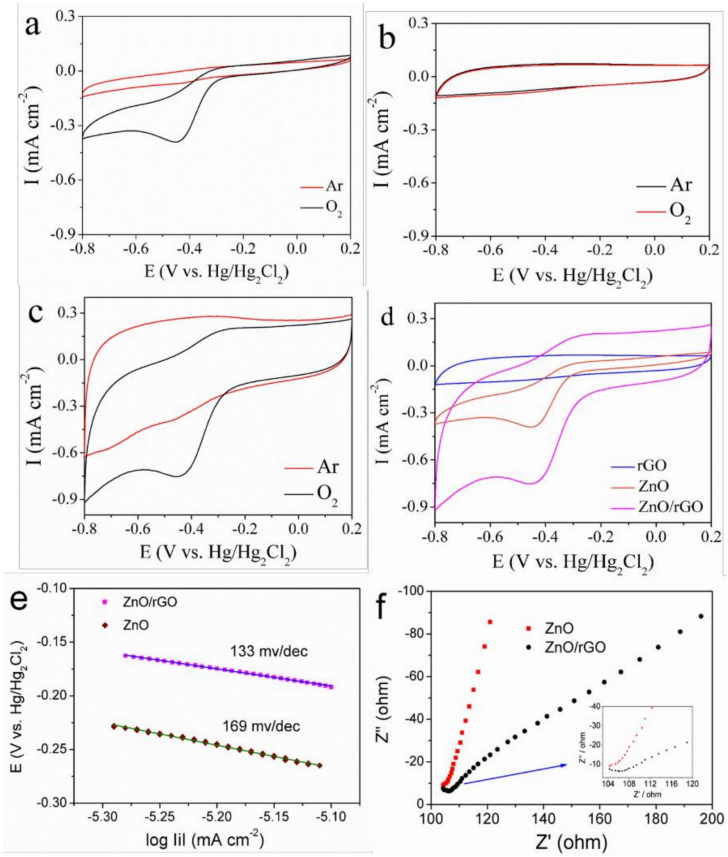

Figure 3. Cyclic voltammograms of (**a**) ZnO, (**b**) rGO and (**c**) ZnO/rGO in Ar and O_2-saturated 0.1 M KOH at 25 °C. (**d**) Comparation of CV tests on ZnO, rGO and ZnO/rGO. Scan rate 5 mV/s. Tafel plots (**e**) and EIS spectrum (**f**) of ZnO and ZnO/rGO.

The exchange current density (i_0) on the two electrodes for ORR is calculated by Equation (1) (Supporting Information) [36]. As shown in Table 1, the i_0 of ZnO and ZnO/rGO is calculated to be 6.76×10^{-7} and 9.21×10^{-5} mA/cm^2, respectively. Obviously, the i_0 of ZnO/rGO is higher than that of ZnO, which is approximate to the commercial Pt/C (10^{-6}~10^{-9} mA/cm^2) [37,38]. The efficient electron transfer between ZnO NPs and rGO nanosheets would result in a high exchange current density and positive charge of ZnO/rGO [39]. To further highlight the benefits of rGO, EIS tests of ZnO and ZnO/rGO were performed at a potential of −0.30 V (vs. SCE). As shown in Figure 3f, the semicircle diameter of ZnO/rGO at the high frequency is smaller than that of ZnO, and the charge transfer resistance (R_{ct}) can be evaluated accordingly. Apparently, ZnO/rGO reveals the smaller R_{ct}, succeeded by ZnO. It is evident that rGO nanosheets can facilitate the process of ORR.

Table 1. Calculated value of i_0 for ZnO and ZnO/rGO.

Sample	ZnO	ZnO-rGO
i_0 (mA/cm^2)	6.67×10^{-7}	9.21×10^{-5}

Rotating disc electrode (RDE) measurements of ZnO and ZnO/rGO were conducted to evaluate the electrocatalytic activity. The test of commercial Pt/C is also provided for comparison. As seen in Figure 4a,c,e, at the mixed kinetics-diffusion control region, the three catalysts show a well-defined increased cathodic current density, while in the diffusion-limited region they all show a parallel plateau.

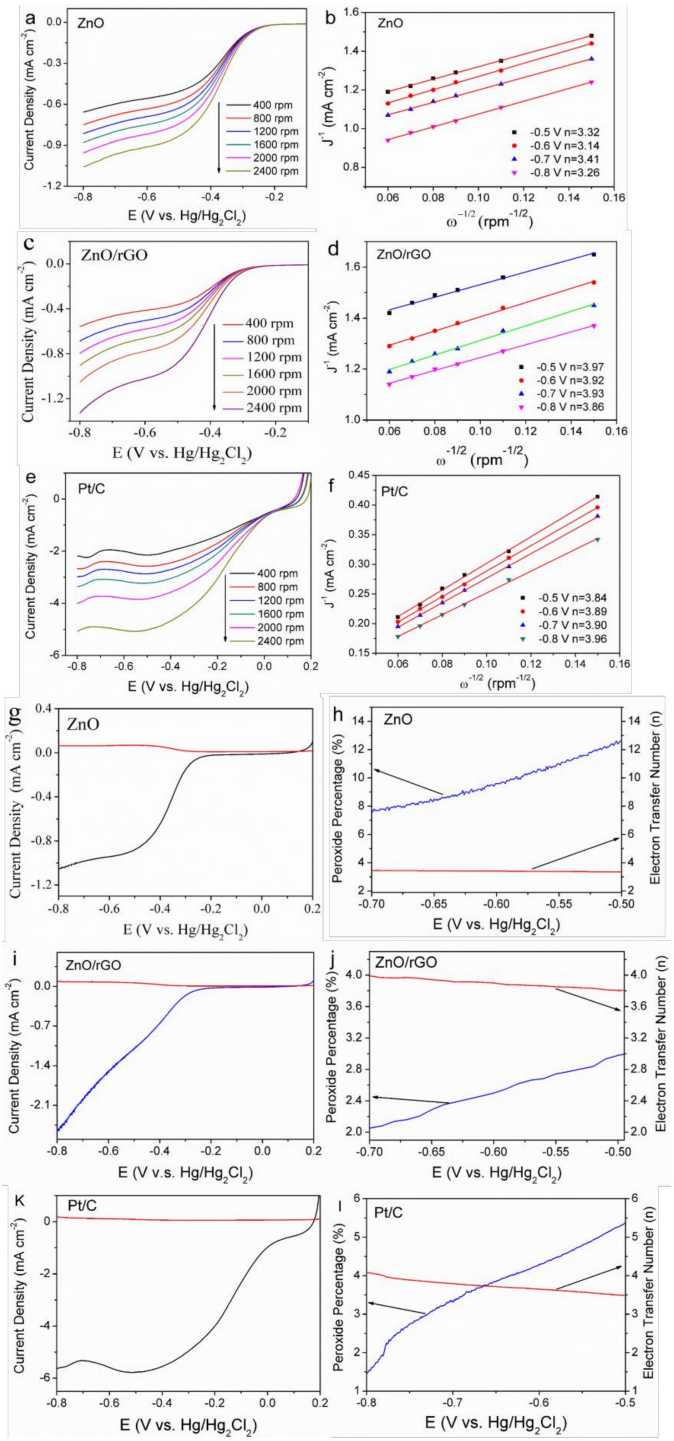

Figure 4. Investigating of ORR Mechanism on catalysts: (**a**,**c**,**e**) RDE profiles of ZnO, ZnO/rGO and commercial Pt/C catalyst, respectively in O_2-saturated 0.1 M KOH solution at various rotation rates ranging from 400 to 2400 rpm, along with (**b**,**d**,**f**) their corresponding Koutecky-Levich plots at different potentials. RRDE profiles (**g**,**i**,**k**) in O_2-saturated 0.1 M KOH solution at a rotation rate of 1600 rpm. Percentage of peroxide and the electron transfer number (**h**,**j**,**l**) at various potentials. Scan rate: 5 mV/s.

Koutecky-Levich theory was employed to unravel the ORR mechanism of ZnO, ZnO/rGO and commercial Pt/C catalyst. Accordingly, the transferred electron numbers (n) can be calculated by Equations (2) and (3) (Supporting Information) [40]. As shown in Figure 4b, the n of ZnO is calculated to be about 3.28 at a potential range of −0.5~−0.8 V, while in Figure 4d,f, the calculated n of ZnO/rGO and Pt/C are about 3.93 and 3.90, respectively. This result indicates that the ORR on ZnO/rGO and Pt/C electrode likely follows a 4-electron mechanistic pathway. However, the ORR catalyzed by ZnO runs in a mixed 2- and 4-electron mechanistic fashion [41]. Rotating ring disc electrode (RRDE) measurements are conducted to probe the exact ORR mechanism of the three catalysts. Figure 4g,i,k show the ring and disk currents of ZnO, ZnO/rGO and Pt/C, recorded at 1600 rpm at a scan rate of 5 mV/s in 0.1 M KOH solution. Compared with ZnO, ZnO/rGO exhibits a higher disk current, while a less amount of intermediate by-products during ORR process. But the disk current of ZnO/rGO is still smaller than that of Pt/C catalyst. Furthermore, the ORR percentage of peroxide species and electron transfer numbers of the three samples were calculated from Equations (4) and (5) (Supporting Information) [42]. Figure 4h,j,l show the obtained results. In Figure 4h, the measured H_2O_2 yield on ZnO electrode is lower than 13%. Specifically, the average electron transfer numbers is found to vary between 3.1 and 3.4, indicating that the ORR of ZnO electrode proceeds via both 2- and 4-electron transfer pathways, while, the H_2O_2 yield on ZnO/rGO electrode is lower than 3%, accordingly, the average electron transfer numbers is found to vary between 3.9 and 4.0, indicating a 4-electron process of ORR. The H_2O_2 yield on Pt/C electrode is lower than 6%, and the average electron transfer numbers is found to vary between 3.5 and 4.1. These results are clearly shown in Figure 5a, suggest that the ORR catalyzed by ZnO/rGO is mainly follows a 4-electron process by directly forming hydroxyl species as the final products, which is similar to that of commercial Pt/C catalyst.

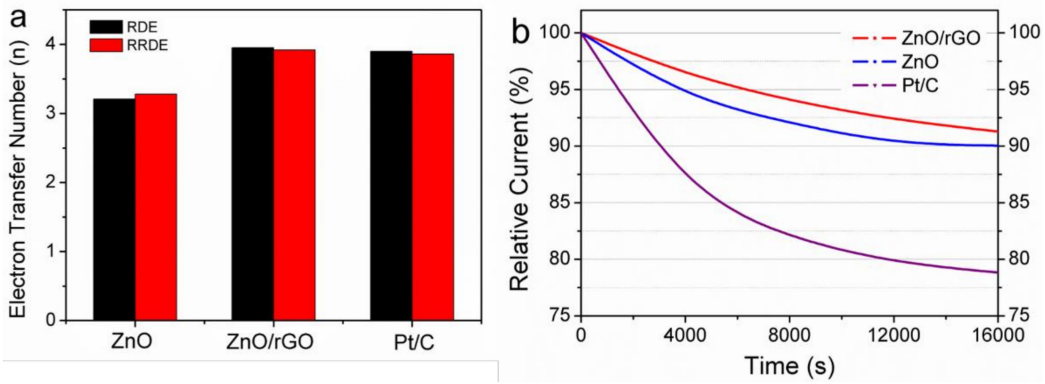

Figure 5. (**a**) Electron transfer number of ZnO, ZnO/rGO and commercial Pt/C catalyst, (**b**) Chronoamperometry of the three catalysts at −0.3 V for 16,000 s.

Chronoamperometry studies are widely used as an effective method to test catalytic stability [43]. Figure 5b shows the chronoamperometric measurement results of ZnO, ZnO/rGO and commercial Pt/C catalyst, by running the ORR for 16,000 s at −0.30 V. It is clearly seen that ZnO/rGO exhibits the highest relative current and a very slow attenuation rate, while commercial Pt/C shows a gradual degradation. For ZnO/rGO hybrid, the loss of catalytic activity results either from the structural changes of the rGO nanosheets or from the degradation of rGO during CV scans. The result clearly suggests the best durability of ZnO/rGO compared with ZnO and commercial Pt/C catalyst.

3. Materials and Methods

Sample Preparation

Graphene oxide (GO) was prepared by a modified Hummers method in our laboratory [44,45], as illustrated in Scheme 1. The ZnO/rGO hybrid was synthesized by a facile hydrothermal method. GO (6 mL, 6 g/L) was added dropwise into the mixture of sodium hydroxide and zinc nitrate

hexahydrate ($Zn(NO_3)_2 \cdot 6H_2O$). After magnetic stirring for 10 min, absolute ethyl alcohol and ethylene glycol were added into this mixture. The obtained solution was placed in a Teflon liner that was sealed in a stainless cylinder and kept at 180 °C for 24 h. After naturally cooling down, the precipitates formed were collected, washed with ethanol and deionized water. Finally, the obtained powder was fully dried at 60–80 °C. Thus 0.80 g of ZnO/rGO was obtained, and the yield of reaction was calculated to be about 94%. Moreover, ZnO catalyst and rGO catalyst were also prepared for comparison, under the same conditions.

Scheme 1. Synthesis procedure of ZnO/rGO hybrid.

4. Conclusions

In summary, we have synthesized a ZnO/rGO hybrid through a facile hydrothermal process. The obtained ZnO/rGO catalyst exhibits high cathodic current density and positive onset potential for ORR in alkaline media, due to the enhanced electron transfer kinetics resulting from the synergetic effect between ZnO NPs and rGO nanosheets. The electron transfer numbers at ZnO/rGO electrode during the ORR process is calculated to be 3.93, indicating a 4-electron mechanistic pathway from O_2 to H_2O. Besides, compared to commercial Pt/C catalyst, ZnO/rGO electrode also shows superior fuel durability, therefore, the ZnO/rGO hybrid is expected to have great potential as an effective noble-metal-free and low-cost catalyst for ORR.

Supplementary Materials: The supplementary materials are available online.

Author Contributions: Writing-original draft: J.Y. Writing-review & editing: J.Y., T.H., Z.J., M.S., C.T.

Funding: Financial support for this work is provided by A Project of Shandong Province Higher Educational Science and Technology Program (J17KA094), Scientific Research Fund of University of Jinan (XBS1644), Science Development Project of Shandong Provincial (2017GGX40115 and 2016GGX102038), Shandong Natural Science Foundation (No. ZR2017QB009 and ZR2018MB036).

Conflicts of Interest: The authors declare no conflicts of interest.

References

1. Pendashteh, A.; Palma, J.; Anderson, M.; Marcilla, R. $NiCoMnO_4$ nanoparticles on *N*-doped graphene: Highly efficient bifunctional electrocatalyst for oxygen reduction/evolution reactions. *Appl. Catal. B Environ.* **2017**, *201*, 241–252. [CrossRef]
2. Chatterjee, K.; Ashokkumar, M.; Gullapalli, H.; Gong, Y.; Vajtai, R.; Thanikaivelan, P.; Ajayan, P.M. Nitrogen-rich carbon nano-onions for oxygen reduction reaction. *Carbon* **2018**, *130*, 645–651. [CrossRef]
3. Debe, M.K. Electrocatalyst approaches and challenges for automotive fuel cells. *Nature* **2012**, *486*, 43–51. [CrossRef] [PubMed]
4. Gewirth, A.A.; Thorum, M.S. Electroreduction of dioxygen for fuel-cell applications: Materials and challenges. *ChemInform* **2010**, *49*, 3557–3566. [CrossRef] [PubMed]
5. Jia, Q.; Zhao, Z.; Cao, L.; Li, J.; Ghoshal, S.; Davies, V.; Stavitski, E.; Attenkofer, K.; Liu, Z.; Li, M.; et al. Roles of mo surface dopants in enhancing the ORR performance of octahedral PtNi nanoparticles. *Nano Lett.* **2018**, *18*, 798–804. [CrossRef] [PubMed]
6. Geng, Z.; Wang, H.; Wang, R.; Zhang, P.; Lang, J.; Wang, C. Facile synthesis of hierarchical porous carbon for supercapacitor with enhanced electrochemical performance. *Mater. Lett.* **2016**, *182*, 1–5. [CrossRef]
7. Xu, J.J.; Yang, J. Nanostructured amorphous manganese oxide cryogel as a high-rate lithium intercalation host. *Electrochem. Commun.* **2003**, *5*, 230–235. [CrossRef]

8. Cheng, F.; Su, Y.; Liang, J.; Tao, Z.; Chen, J. MnO_2-Based Nanostructures as Catalysts for Electrochemical Oxygen Reduction in Alkaline Media. *Chem. Mater.* **2010**, *22*, 898–905. [CrossRef]
9. Feng, X.; Chen, N.; Zhang, Y.; Yan, Z.; Liu, X.; Ma, Y.; Shen, Q.; Wang, L.; Huang, W. The self-assembly of shape controlled functionalized graphene-MnO_2 composites for application as supercapacitors. *J. Mater. Chem. A* **2014**, *2*, 9178–9184. [CrossRef]
10. Hossen, M.M.; Artyushkova, K.; Atanassov, P.; Serov, A. Synthesis and characterization of high performing Fe-N-C catalyst for oxygen reduction reaction (ORR) in alkaline exchange membrane fuel cells. *J. Power Sources* **2018**, *375*, 214–221. [CrossRef]
11. Liang, Y.; Wang, H.; Zhou, J.; Li, Y.; Jian, W.; Regier, T.; Dai, H. Covalent hybrid of spinel manganese-cobalt oxide and graphene as advanced oxygen reduction electrocatalysts. *J. Am. Chem. Soc.* **2012**, *134*, 3517–3523. [CrossRef]
12. Kannan, M.V.; Gnana Kumar, G. Current status, key challenges and its solutions in the design and development of graphene based ORR catalysts for the microbial fuel cell applications. *Biosens. Bioelectron.* **2016**, *77*, 1208–1220. [CrossRef]
13. Bassetto, V.C.; Xiao, J.; Oveisi, E.; Amstutz, V.; Liu, B.; Girault, H.H.; Lesch, A. Rapid inkjet printing of high catalytic activity Co_3O_4/N-rGO layers for oxygen reduction reaction. *Appl. Catal. A General* **2018**, *563*, 9–17. [CrossRef]
14. Li, J.; Wang, Q.; Liu, K.; Jiang, J.; Qian, D.; Li, J.; Chen, Z. An extremely facile route to Co@CoO/N-RGO/AB with an enhanced electrocatalytic activity for ORR. *Mater. Lett.* **2017**, *186*, 189–192. [CrossRef]
15. Yao, T.; Guo, X.; Qin, S.; Xia, F.; Li, Q.; Li, Y.; Chen, Q.; Li, J.; He, D. Effect of rGO coating on interconnected Co_3O_4 nanosheets and improved supercapacitive behavior of Co_3O_4/rGO/NF architecture. *Nano-Micro Lett.* **2017**, *9*, 38. [CrossRef] [PubMed]
16. Hu, Z.; Zhou, X.; Lu, Y.; Jv, R.; Liu, Y.; Li, N.; Chen, S. $CoMn_2O_4$ doped reduced graphene oxide as an effective cathodic electrocatalyst for ORR in microbial fuel cells. *Electrochim. Acta* **2019**, *296*, 214–223. [CrossRef]
17. Yu, J.; Liu, Z.; Zhai, L.; Huang, T.; Han, J. Reduced graphene oxide supported TiO_2 as high performance catalysts for oxygen reduction reaction. *Int. J. Hydrogen Energy* **2016**, *41*, 3436–3445. [CrossRef]
18. Guo, D.; Dou, S.; Li, X.; Xu, J.; Wang, S.; Lai, L.; Liu, H.K.; Ma, J.; Dou, S.X. Hierarchical MnO_2/rGO hybrid nanosheets as an efficient electrocatalyst for the oxygen reduction reaction. *Int. J. Hydrogen Energy* **2016**, *41*, 5260–5268. [CrossRef]
19. Yan, Z.; Qi, H.; Bai, X.; Huang, K.; Chen, Y.-R.; Wang, Q. Mn doping of cobalt oxynitride coupled with *N*-rGO nanosheets hybrid as a highly efficient electrocatalyst for oxygen reduction and oxygen evolution reaction. *Electrochim. Acta* **2018**, *283*, 548–559. [CrossRef]
20. Nasser, R.; Othmen, W.B.H.; Elhouichet, H.; Férid, M. Preparation, characterization of Sb-doped ZnO nanocrystals and their excellent solar light driven photocatalytic activity. *Appl. Surf. Sci.* **2017**, *393*, 486–495. [CrossRef]
21. Sun, Y.; Shen, Z.; Xin, S.; Ma, L.; Xiao, C.; Ding, S.; Li, F.; Gao, G. Ultrafine Co-doped ZnO nanoparticles on reduced graphene oxide as an efficient electrocatalyst for oxygen reduction reaction. *Electrochim. Acta* **2017**, *224*, 561–570. [CrossRef]
22. Yang, J.; Jia, H.; Lv, X.; Wang, Y. Facile preparation of urchin-like ZnO nanostructures and their photocatalytic performance. *Ceram. Int.* **2016**, *42*, 12409–12413. [CrossRef]
23. Zhang, Y.; Feng, T.; Zhou, X.; Pei, Q.; Hao, T.; Zhang, W.; Wu, S.; Mao, H.; Song, X.-M. Facile preparation of one dimension ZnO/chalcogenide semiconductor heterostructure for efficient photoelectrochemical water splitting. *J. Alloy. Compd.* **2016**, *685*, 581–586. [CrossRef]
24. Zhang, Z.; Song, X.; Chen, Y.; She, J.; Deng, S.; Xu, N.; Chen, J. Controllable preparation of 1-D and dendritic ZnO nanowires and their large area field-emission properties. *J. Alloy. Compd.* **2017**, *690*, 304–314. [CrossRef]
25. Wang, Y.-Y.; Zhou, G.-Q.; Guo, J.; Liu, T.-Q. Controllable preparation of porous ZnO microspheres with a niosome soft template and their photocatalytic properties. *Ceram. Int.* **2016**, *42*, 12467–12474. [CrossRef]
26. Zhou, J.; Xiao, H.; Zhou, B.; Huang, F.; Zhou, S.; Xiao, W.; Wang, D. Hierarchical MoS_2-rGO nanosheets with high MoS2 loading with enhanced electro-catalytic performance. *Appl. Surf. Sci.* **2015**, *358*, 152–158. [CrossRef]
27. Zuo, L.-X.; Wang, W.-J.; Song, R.-B.; Lv, J.-J.; Jiang, L.-P.; Zhu, J.-J. NaCl crystal tuning nitrogen self-doped porous graphitic carbon nanosheets for efficient oxygen reduction. *ACS Sustain Chem. Eng.* **2017**, *5*, 10275–10282. [CrossRef]

28. Motaung, D.E.; Mhlongo, G.H.; Nkosi, S.S.; Malgas, G.F.; Mwakikunga, B.W.; Coetsee, E.; Swart, H.C.; Abdallah, H.M.; Moyo, T.; Ray, S.S. Shape-selective dependence of room temperature ferromagnetism induced by hierarchical ZnO nanostructures. *ACS Appl. Mater. Interfaces* **2014**, *6*, 8981–8995. [CrossRef]
29. Park, S.M.; Ikegami, T.; Ebihara, K. Effects of substrate temperature on the properties of Ga-doped ZnO by pulsed laser deposition. *Thin Solid Films* **2006**, *513*, 90–94. [CrossRef]
30. Chandraboss, V.L.; Kamalakkannan, J.; Prabha, S.; Senthilvelan, S. An efficient removal of methyl violet from aqueous solution by an AC-Bi/ZnO nanocomposite material. *RSC Adv.* **2015**, *5*, 479–490. [CrossRef]
31. Hong, Y.; Tian, C.; Jiang, B.; Wu, A.; Zhang, Q.; Tian, G.; Fu, H. Facile synthesis of sheet-like ZnO assembly composed of small ZnO particles for highly efficient photocatalysis. *J. Mater. Chem. A* **2013**, *1*, 5700–5708. [CrossRef]
32. Khandelwal, M.; Chandrasekaran, S.; Hur, S.H.; Chung, J.S. Chemically controlled in-situ growth of cobalt oxide microspheres on *N*,*S*-co-doped reduced graphene oxide as an efficient electrocatalyst for oxygen reduction reaction. *J. Power Sources* **2018**, *407*, 70–83. [CrossRef]
33. Yan, Z.; Dai, C.; Lv, X.; Zhang, M.; Zhao, X.; Xie, J. Iron promoted nitrogen doped porous graphite for efficient oxygen reduction reaction in alkaline and acidic media. *J. Alloy. Compd.* **2019**, *773*, 819–827. [CrossRef]
34. Luo, Q.; Yang, X.; Zhao, X.; Wang, D.; Yin, R.; Li, X.; An, J. Facile preparation of well-dispersed ZnO/cyclized polyacrylonitrile nanocomposites with highly enhanced visible-light photocatalytic activity. *Appl. Catal. B Environ.* **2017**, *204*, 304–315. [CrossRef]
35. Bian, W.; Yang, Z.; Strasser, P.; Yang, R. A $CoFe_2O_4$/graphene nanohybrid as an efficient bi-functional electrocatalyst for oxygen reduction and oxygen evolution. *J. Power Sources* **2014**, *250*, 196–203. [CrossRef]
36. Camacho, B.R.; Morais, C.; Valenzuela, M.A.; Alonso-Vante, N. Enhancing oxygen reduction reaction activity and stability of platinum via oxide-carbon composites. *Catal. Today* **2013**, *202*, 36–43. [CrossRef]
37. Hung, T.F.; Bei, W.; Tsai, C.W.; Tu, M.H.; Wang, G.X.; Liu, R.S.; Tsai, D.P.; Lo, M.Y.; Shy, D.S.; Xing, X.K. Sulfonation of graphene nanosheet-supported platinum via a simple thermal-treatment toward its oxygen reduction activity in acid medium. *Int. J. Hydrogen Energy* **2012**, *37*, 14205–14210. [CrossRef]
38. He, C.; Tao, J.; Shen, P.K. Solid synthesis of ultrathin palladium and its alloys' nanosheets on RGO with high catalytic activity for oxygen reduction reaction. *ACS Catal.* **2018**, *8*, 910–919. [CrossRef]
39. Wang, S.; Yu, D.; Dai, L. Polyelectrolyte functionalized carbon nanotubes as efficient metal-free electrocatalysts for oxygen reduction. *J. Am. Chem. Soc.* **2011**, *133*, 5182–5185. [CrossRef]
40. Kakaei, K.; Hasanpour, K. Synthesis of graphene oxide nanosheets by electrochemical exfoliation of graphite in cetyltrimethylammonium bromide and its application for oxygen reduction. *J. Mater. Chem. A* **2014**, *2*, 15428–15436. [CrossRef]
41. Kumar, S.; Kumar, D.; Kishore, B.; Ranganatha, S.; Munichandraiah, N.; Venkataramanan, N.S. Electrochemical investigations of Co_3Fe-RGO as a bifunctional catalyst for oxygen reduction and evolution reactions in alkaline media. *Appl. Surf. Sci.* **2017**, *418*, 79–86. [CrossRef]
42. Hibino, T.; Kobayashi, K.; Heo, P. Oxygen reduction reaction over nitrogen-doped graphene oxide cathodes in acid and alkaline fuel cells at intermediate temperatures. *Electrochim. Acta* **2013**, *112*, 82–89. [CrossRef]
43. Ahmed, M.S.; Lee, D.W.; Kim, Y.B. Graphene supported silver nanocrystals preparation for efficient oxygen reduction in alkaline fuel cells. *J. Electrochem. Soc.* **2016**, *163*, F1169–F1176. [CrossRef]
44. Wang, G.; Shen, X.; Wang, B.; Yao, J.; Park, J. Synthesis and characterisation of hydrophilic and organophilic graphene nanosheets. *Carbon* **2009**, *47*, 1359–1364. [CrossRef]
45. Hu, J.; Zhang, F. Self-assembled fabrication and flame-retardant properties of reduced graphene oxide/waterborne polyurethane nanocomposites. *J. Therm. Anal. Calorim.* **2014**, *118*, 1561–1568. [CrossRef]

Sample Availability: Samples are available from the authors.